

## Electron capture from a directed Stark-Rydberg state: Fore-and-aft ratios

D. M. Homan, O. P. Makarov, O. P. Sorokina, and K. B. MacAdam

*Department of Physics and Astronomy, University of Kentucky, Lexington, Kentucky 40506-0055*

M. F. V. Lundsgaard

*Debye Institute, University of Utrecht, Princetonplein 5, 3508 TA Utrecht, The Netherlands*

C. D. Lin

*Department of Physics, Kansas State University, Manhattan, Kansas 66506*

N. Toshima

*Institute of Applied Physics, University of Tsukuba, Tsukuba, Ibaraki 305, Japan*

(Received 30 June 1998)

Electron capture by  $\text{Cs}^+$ ,  $\text{K}^+$ , or  $\text{Li}^+$  from a Na Rydberg target in an extreme Stark state of  $n=24$ ,  $m=0$  has been measured and compared with both a classical and a quantal calculation as a function of the reduced velocity  $\tilde{v}=0.15-1.6$ . Peaks and shoulders are found at  $\tilde{v}=0.25$ ,  $0.5$ , and  $1.0$  in the ratio of the measured capture cross sections for electronic charge polarization antiparallel and parallel to the ion-beam direction. A close-coupling calculation reveals similar features in the total capture cross sections near those same scaled velocities. A classical trajectory calculation attributes this structure to *swapping* of the electron between the two positive charge centers as they pass one another during the collision. The total classical capture cross section of a Rydberg atom having an upstream-directed charge distribution is shown to be the sum of five-and-greater-swap, three-swap, and one-swap contributions, which result in the structure near  $\tilde{v}=0.25$ ,  $0.5$ , and  $1.0$ , respectively. [S1050-2947(98)03312-5]

PACS number(s): 34.10.+x, 34.60.+z, 34.70.+e

### I. INTRODUCTION

Experiments that measure electron capture by heavy singly charged ions from oriented and aligned Rydberg [1-7] and laser-aligned [8,9] low- $n$  state targets have revealed much about the Coulomb three-body dynamics of electron capture and have demonstrated that velocity matching between the projectile and electron is an important feature of these rearrangement collisions, as known since the early days of quantum mechanics [10]. Both classical [11-19] and quantal [20-26] theories have been developed to model these collisions. The theories have demonstrated the importance of velocity matching and the classical formulations have recently revealed another phenomenon in electron capture that is significant near  $\tilde{v}=v_{\text{ion}}/v_{\text{Bohr}}=1$  [12,14,19], as follows. It was shown by Homan, Cavagnero, and Harmin [14,17] that a spatial mechanism called three-swap capture, similar to the high-velocity Thomas capture mechanism [27,28] in that the electron interacts successively with both the projectile and the target, became important at  $\tilde{v}<1.0$  [5,14,17,29]. A *swap* is a single passage of the pointlike electron across the moving midplane that divides the two heavy positive centers. To study this low-velocity phenomenon we have measured electron capture by a singly charged ion from a Rydberg atom prepared in a top Stark state near the matching velocity, which enhances its effect. By means of an external electric field directed parallel or antiparallel to the ion beam we direct the atom's electric dipole moment  $\mathbf{d}_e=\frac{3}{2}n\langle\mathbf{A}\rangle$  either antiparallel or parallel to the ion beam, respectively, where  $\mathbf{A}$  is the Runge-Lenz vector [30]. Since

the contribution of velocity matching alone to capture would be identical for an upstream-directed (negative-charge polarization angle  $180^\circ$ ) and downstream-directed (polarization angle  $0^\circ$ ) Stark state, based on the state's inherent symmetry in velocity space, any departure from equality of cross sections from these two extreme states would be a signature of a *spatial* phenomenon. We refer to it as *spatial* because it matters *where* the electron is primarily located in the target atom, as opposed to in what direction and how fast it is moving. We have observed peaks and shoulders in the measured ratio of the upstream and downstream cross sections, the *fore-and-aft capture ratio*, as a function of reduced velocity near  $\tilde{v}=1.0$ ,  $0.5$ , and  $0.25$ . These features are predicted in both a close-coupling (CC) calculation by Lundsgaard and Lin [31,32] and by classical-trajectory Monte Carlo (CTMC) theory [17]. The close-coupling calculation of a proton incident on atomic hydrogen in Stark levels of  $n=4$  is in good quantitative agreement with the scaled velocity dependence of the present measurements. The CTMC calculation attributes this observed structure to one-, three-, and higher-order odd- $n$  swaps. The classical calculation is also in good qualitative agreement with the measurement. It has been demonstrated in Ref. [14] by examination of trajectories that the one-swap contribution is direct capture and the three-swap contribution in the high-velocity limit is a double scattering of the electron first by the projectile and then by the target nucleus resulting in capture of the electron by the incident projectile. This is the Thomas capture mechanism [27] classically or the second-Born approximation [28,33] quantum mechanically. The empirical results along with the classical explanation for the structure have greatly enhanced

our knowledge of this three-body system in the correspondence principle regime near the reduced velocity  $\tilde{v} = 1$ .

The oscillations seen in the measured capture cross section at low energies may also have a quantum explanation similar to symmetric resonance charge transfer. This phenomenon is observed in homonuclear collisions, for example, between a proton and a hydrogen atom in a low- $n$  state. Here the oscillation is clearly seen in the charge-transfer probability as a function of the impact parameter [34] and is attributed to the oscillation of the electronic wave function between the target and projectile during the collision. This oscillation in the probability, however, is suppressed in low- $n$  *total-capture* cross sections because of averaging, although oscillations in total cross sections have been observed and analyzed [35,36]. The resulting nearly constant capture cross section (at low energies) contrasts starkly with the structure seen in our measurements. Avakov *et al.* [37] have obtained suggestive oscillations in proton-alkali-metal-atom capture reactions from calculations based on the Faddeev three-body equations written in the Alt-Grassberger-Sandhas form. More recently Schultz *et al.* [38] have proposed that oscillatory structures are more universal than initially supposed and may be attributed to a collective coherent phenomenon involving more than two molecular levels. Hansen *et al.* [39] have demonstrated related features in minimal-basis-set atomic-orbital calculations of  $p + \text{H}(1s)$  and  $\alpha + \text{H}(1s)$  collisions, where structures apparently result from a shift from direct excitation at high velocity to two-center molecular effects at low velocity.

In Sec. II we give the experimental details. In Sec. III a classical and a quantal description of the heavy-ion-atom collision are briefly presented. In Sec. IV the experimental results are described and compared with the theories. In Sec. V we give concluding remarks and suggest future objectives.

## II. EXPERIMENTAL METHOD

### A. Interaction region

The experimental apparatus is shown in Fig. 1. The interaction region is the interior of a *Stark barrel* [40]. The Stark barrel (SB) is an arrangement of electrodes and associated electronics that creates an electric field initially parallel ( $0^\circ$ ) or antiparallel ( $180^\circ$ ) to the ion beam and then in  $2 \mu\text{s}$  smoothly alters it to a smaller electric field in any direction in the plane of the ion and target beams. In this paper we are only concerned with the electric fields parallel or antiparallel to the ion beam and not with field rotation, but in a separate paper the full two-dimensional capabilities of the SB will be discussed and exploited [41]. Furthermore, we will look specifically at the extreme Stark states of the target in this electric field, which leave the electron cloud of the target directed maximally either towards or away from the approaching ion beam.

The magnitudes and directions of the initial Stark field  $\mathbf{F}_S$  and final barrel field  $\mathbf{F}_b$  were chosen in view of experimental constraints. The final electric field  $\mathbf{F}_b$  was chosen in the range  $0.5\text{--}2 \text{ V cm}^{-1}$  to ensure that the ion beam would not be deflected or defocused significantly as it entered and exited the barrel. It was necessary to create an electric field  $\mathbf{F}_S$  initially both large and parallel or antiparallel to the ion

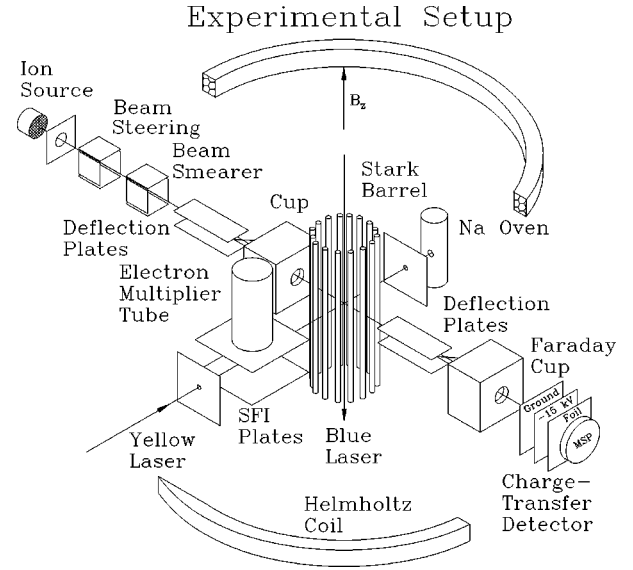


FIG. 1. Schematic of the experimental setup for the measurement of the total capture cross section in ion impact with Na(24 top).

beam for two reasons. First, we had to ensure that we were populating mostly the top Stark level of the  $n=24$  manifold, indicated by the cross in Fig. 2. For this reason the linear Stark splitting ( $0.5 \text{ cm}^{-1}$ ) had to be greater than the linewidth of the blue dye laser, which is typically  $0.15 \text{ cm}^{-1}$  or 4.5 GHz. Second, we needed to ensure that we were populating mostly the  $m=0$  azimuthal quantum number with respect to the ion beam and for this reason both the initial electric field and the planes of linear polarization of laser beams had to be parallel to the ion beam.

According to Harmin [42], the condition for adiabatic evolution of the  $n=24, m=0$  top Stark state of Na during the transition from  $\mathbf{F}_S$  to  $\mathbf{F}_b$  is  $\dot{F} \leq 10^4 \text{ V cm}^{-1} \mu\text{s}^{-1}$ . A typical  $\dot{F}$  in the barrel is  $100 \text{ V cm}^{-1} \mu\text{s}^{-1}$ , which is extremely adiabatic. The wave function is essentially independent of the electric field, as in the case of a parabolic state of H. We measured the charge-transfer cross section at a given  $\tilde{v}$  as a

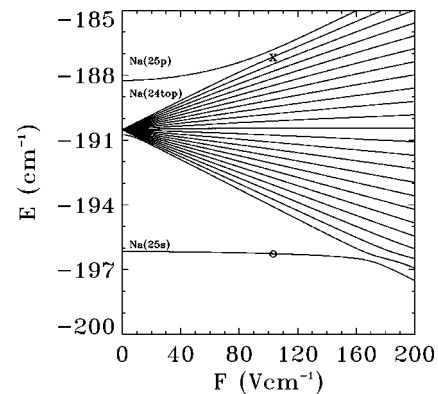


FIG. 2. Na Stark energy levels near  $n=24$ . The Na(24 top) state is excited near  $150 \text{ V cm}^{-1}$  and then switched adiabatically down to  $0.5\text{--}2 \text{ V cm}^{-1}$  without rotation or zero crossing of the field. Measurements of capture from the Na(25s) state are interspersed for normalization.

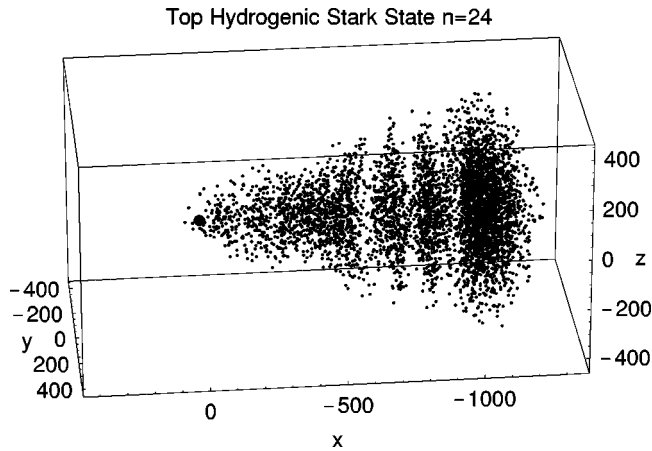


FIG. 3. Perspective representation of the Na(24 top) wave function.

function of  $\hat{F}$  and found our results to be constant within the range  $33 \leq \hat{F} \leq 200 \text{ V cm}^{-1} \mu\text{s}^{-1}$  that was available to us.

The Na target cloud is prepared in the atomic beam about 3 mm from its intersection with the alkali-metal ion beam in the presence of the Stark electric field,  $\mathbf{F}_S = 150 - 200 \text{ V cm}^{-1}$  either parallel or antiparallel to the ion beam. The top Stark state of the  $n = 24$  linear manifold is populated by a 20-Hz two-step pulsed laser excitation  $3^2S_{1/2} \rightarrow 3^2P_{3/2} \rightarrow \text{Na}(24 \text{ top})$ . The necessary laser wavelengths are 589 nm (yellow) and 410 nm (blue), respectively. A perspective representation of  $|\psi|^2$  for a Na(24 top) wave function  $\psi$  is shown in Fig. 3, where it is seen that the electron probability, represented by the density of dots in space, is directed away from the nucleus in the shape of a filled cone. The cone widens in the direction of the external electric field  $\mathbf{F}$  away from the nucleus and thus  $\mathbf{F}$  serves to orient the electron distribution in space. In an oppositely directed field the electron probability density in configuration space is exactly reversed. The Stark field is electronically switched adiabatically in approximately  $2 \mu\text{s}$  to an electric field  $\mathbf{F}_b = 0.5 - 2 \text{ V cm}^{-1}$  parallel to  $\mathbf{F}_S$ . The target cloud of *directed* Rydberg atoms drifts towards the ion beam at roughly  $0.7 \text{ mm } \mu\text{s}^{-1}$  during the electric-field transition so that when the target volume intersects the ion beam the electric fields have stabilized. We refer to these as directed states, rather than aligned states, to emphasize their off-center electronic asymmetry and definite axial direction without treading upon the technical meaning of alignment [43].

### B. Beams

A crossed-beam collision geometry is used in this experiment. A thermal beam of Na atoms is extracted from a  $200^\circ\text{C}$  oven. After the Na beam passes through two 3-mm apertures at its thermal velocity, it enters the SB, where, 2.1 mm or  $3 \mu\text{s}$  before it reaches the center of the SB, it is exposed to an 8-ns pulsed two-step laser excitation (at a 20-Hz repetition rate) in the presence of  $\mathbf{F}_S$  to populate the Na(24 top) state. Next  $\mathbf{F}_S$  is switched to  $\mathbf{F}_b$  in  $2 \mu\text{s}$ , and the target state evolves adiabatically with it. The prepared target-state atoms (about 1000 atoms per pulse) then collide with the ion beam in the presence of  $\mathbf{F}_b$  and charge transfer occurs. Most of the unreacted target Rydberg atoms exit the

SB into a pair of condenser plates, where  $40 \mu\text{s}$  after the laser flash they undergo state-selective field ionization (SFI) in a pulsed electric field. The SFI signal detected in an electron multiplier tube is used to monitor the target state and to normalize the capture cross section.

The (0.5–5) nA alkali-metal ion beam ( $\text{Cs}^+$ ,  $\text{K}^+$ , or  $\text{Li}^+$ ) is extracted from a thermionic-emitter ion source [44] and accelerated to  $E = 50 - 2000 \text{ eV}$ . This corresponds to a reduced velocity range  $\tilde{v} = 0.00635n^* \sqrt{E(\text{eV})/M(\text{amu})} = 0.15 - 2.5$ , depending on the mass  $M$  of the ion. [ $n^*$  is the quantum-defect corrected principal quantum number of the initial Rydberg state. For the 24 top state  $n^* = n$  and for Na( $ns$ ) states  $n^* = n - 1.65$  [45].] The ion beam is steered by a set of vertical and horizontal deflectors, which are used to maximize the ion current measured in a Faraday cup beyond the SB. A second set of deflectors is used to randomly deflect the ion beam to average out possible nonuniform ion density [46]. This random deflection (“smearing”) is needed at low acceleration voltages when the ion beam is poorly focused and may not be homogeneous. Before reaching the SB the ion beam is deflected into an upstream Faraday cup except during a  $400\text{-}\mu\text{s}$  period while the SB is at a small  $\mathbf{F}_b$ . This is done to avoid charging of surfaces in the barrel during long periods of operation and to accurately measure the ion current in the downstream Faraday cup when  $\mathbf{F}_b$  is applied to the SB. A 3-mm aperture is placed before and after the SB to collimate the ion beam.

At the center of the SB the ion beam interacts with the target beam and some of the ions are neutralized by charge transfer. Only two or fewer captures take place in the target per laser flash. The ions and the neutral atoms then exit the SB and enter a region of constant transverse electric field, which deflects the ions into the downstream Faraday cup where the beam-current pulse is measured in a fast current sampler. (The small deflection field, obtained by applying approximately 10% of the accelerating voltage across plates separated by 1 cm, would ionize capture products in very high Rydberg states. Direct tests, in which the strength of the deflecting field was varied widely, showed that the total capture signal at ion velocity  $\tilde{v} = 0.8$  was unaffected by the deflection fields at the chosen operating point.) The neutral capture products, which are not deflected, continue on to the charge-transfer detector [1], arriving in  $5 - 15 \mu\text{s}$ . The detector registers Rydberg-atom arrivals for  $n > 15$ , limited by its 15-kV/cm stripping field, and  $n$  less than approximately 40, limited by prestripping in deflection fields. The charge-transfer counts are recorded in both 5- and  $10\text{-}\mu\text{s}$  windows after their first appearance. Use of two electronic counting windows allows us to detect whether the target states are being progressively altered during its exposure by processes such as blackbody radiation, ion-Rydberg collisions, or Rydberg-background-gas collisions. We observe no difference in relative cross section results between short and long windows. We also observe a small amount of contamination from unwanted alkali-atom ions from the thermionic emitter in our ion beam and have used their differing flight times between the interaction region and the detector to eliminate counts that result from them.

Three projectile ions were used to measure charge transfer over the largest possible range of reduced velocity.  $\text{Cs}^+$  was

used to cover  $\tilde{v}=0.15-0.55$ ,  $K^+$  was used to cover  $\tilde{v}=0.3-1.05$ , and  $Li^+$  was used to cover  $\tilde{v}=0.9-1.6$ . In the overlapping regions, the ratios of the fore-and-aft cross-section ratios were similar between the different ion species. The cross section becomes increasingly difficult to measure for each ion at its lowest energy since the ion current falls off rapidly with decreased acceleration voltage. In the case of  $Li^+$  the cross section also becomes increasingly difficult to measure at  $\tilde{v}\geq 1.6$ , for the cross section decreases precipitously at  $\tilde{v}\geq 1$  [28].

### C. Measurement procedure

To measure the fore-and-aft capture cross-section ratio  $r$ , we first measured the ratio  $r_{180}$  of the Na(24 top) and Na(25s) capture cross sections for the electric field antiparallel to the ion beam as a function of reduced velocity and then repeated this to measure  $r_0$  for the electric field parallel to the ion beam. We ignored the 1% difference in  $\tilde{v}$  at each beam energy  $E$  attributable to the  $s$  state's quantum defect. The Na(25s) state is indicated in Fig. 2 by an open circle. The fore-and-aft ratio  $r$  is the quotient of these two ratios,  $r=r_{180}/r_0$ , which was then independent of the Na(25s) capture cross section and equivalent to the quotient of upstream and downstream cross sections directly. The Na(25s) capture cross section was utilized to cancel out systematic effects due to the deflection or defocusing of the ion beam by the  $(0.5-2)$ -V  $cm^{-1}$  barrel field in its two orientations.

## III. THEORY

We present results of two different theoretical approaches to the present scattering problem in the form of a pure classical and a quantum mechanical model, respectively. Both models have already been discussed in the literature [15,21] and will therefore be described only briefly.

### A. Classical trajectory model

A recently presented model study of charge transfer and ionization channels for ion collisions with circular and elliptic Rydberg atoms [14,17] has led to a clearer understanding of the structures observed in total capture cross sections near  $\tilde{v}=1$  [15–17]. The total capture cross sections were shown as contributions of one-swap, three-swap, and higher-order odd-numbered swaps, where the number of swaps is defined as the number of times the electron crosses the potential saddle between the two ions. In this classical-trajectory (CT) model the target state consists of an electron in a single Keplerian orbit chosen to satisfy the appropriate mean initial conditions [47]. In the present calculation the top Stark level was represented by a single elliptical orbit with an eccentricity of  $e\sim 1$  (actually,  $e=0.995$ ), classical angular momentum perpendicular to the alkali-metal ion beam, and a Runge-Lenz vector parallel (electron charge polarization angle  $180^\circ$ ) or antiparallel ( $0^\circ$ ) to the ion-beam direction.

### B. Quantum-mechanical model: Close coupling

We have also performed CC calculations [48] for protons colliding with  $H(n=4)$  in a general coherent elliptic state

[49]. The calculations were done within the impact-parameter approximation, in which it is assumed that the relative motion of the nuclei follows a straight-line trajectory. Plane-wave electronic translation factors were used. For the target state with eccentricity  $e$  we use the notation  $|n=4,e\rangle$  in the following.

Expressing  $|n=4,e\rangle$  in terms of the usual spherical harmonics  $|nlm\rangle$ , it was shown in Ref. [22] that the cross section for electron capture from  $|n=4,e\rangle$  for any collision geometry may be obtained analytically once the reduced density matrix

$$\rho_{kk'} = \sum_f a_{fk} a_{fk'}^*, \quad (1)$$

is known. Here  $a_{fk}$  is the scattering amplitude for the capture process  $|k\rangle\rightarrow|f\rangle$  and the index  $k$  represents the  $(nlm)$  set of quantum numbers. To obtain the electron-capture cross section in the general case (including the case of a linear Stark state) we thus have to carry out close-coupling calculations for all the  $lm$  substates of the  $n$  manifold.

For the close-coupling calculations presented here we have used a two-center atomic-orbital expansion of the electronic wave function. On both centers all the  $1\leq n\leq 5$  states were included in the basis set. The states themselves were generated from Gaussian-type orbitals [50].

## IV. EXPERIMENTAL AND THEORETICAL RESULTS

The fore-and-aft ratios  $r$  for the combined experimental data of  $Cs^+$ ,  $K^+$ , or  $Li^+$  on Na(24 top) targets are shown in Fig. 4 as solid dots. The experimental error bars are based on estimated statistical errors and run-to-run variations. Each point is an average of ten or more measurements, which span three different occasions. The ratio has distinct features at  $\tilde{v}=0.25, 0.5$ , and  $1.0$ . The experimental results are compared with both CT (open circles) and close-coupling (open squares) calculations for the corresponding hydrogen  $n=24$  and  $n=4$  Stark states, respectively.

The fore-and-aft ratio as a function of  $\tilde{v}$  rises as high as 5.5:1 (at  $\tilde{v}=0.25$ ). As mentioned earlier, this favoring of capture from the upstream-directed Stark state may be attributed to a spatial phenomenon because the upstream- and downstream-directed Stark states have identical electronic momentum distributions. That is, without some role played by the *spatial location* of the electron in the target atom, irrespective of its motion,  $r$  would be identically one. Not only does  $r$  differ from one, it also shows a structure that suggests a theoretical explanation.

The close-coupling calculation agrees well with the measured ratio from  $\tilde{v}=0.5$  to  $1.0$ . The classical calculation describes well the qualitative structure seen in the experiment, but the CTMC ratio is too large by approximately a factor 4. (We attribute this below to a fourfold shortfall of the calculated  $0^\circ$  capture cross section.) Since the cross section at  $0^\circ$  is nearly featureless (see Fig. 5) the CTMC ratio in Fig. 4 was normalized downward for purposes of comparing the structure in  $r$  that primarily originates in the capture at  $180^\circ$ . Both theoretical calculations, however, become large at low reduced velocities due to the fact that  $r$  is the ratio of a large

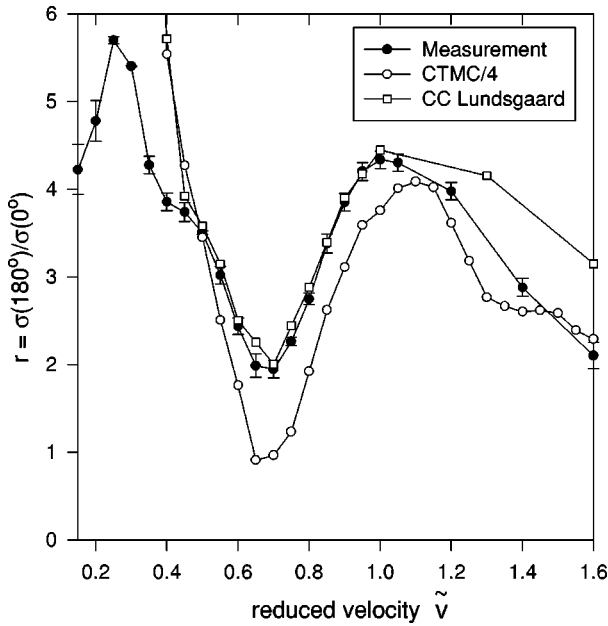


FIG. 4. Velocity dependence of the fore-and-aft ratio of the total capture. The solid circles are the measured values. The open squares are the result of a close-coupling calculation for  $H^+ + H(n)$  for the extreme Stark levels in the  $n = 4$  manifold. The open circles represent a CTMC calculation for  $H^+ + H(e = 0.995)$ , where the ratio is calculated from cases having the Runge-Lenz vector parallel and antiparallel to the ion beam. The CTMC results have been scaled down by a factor 4 (see the text).

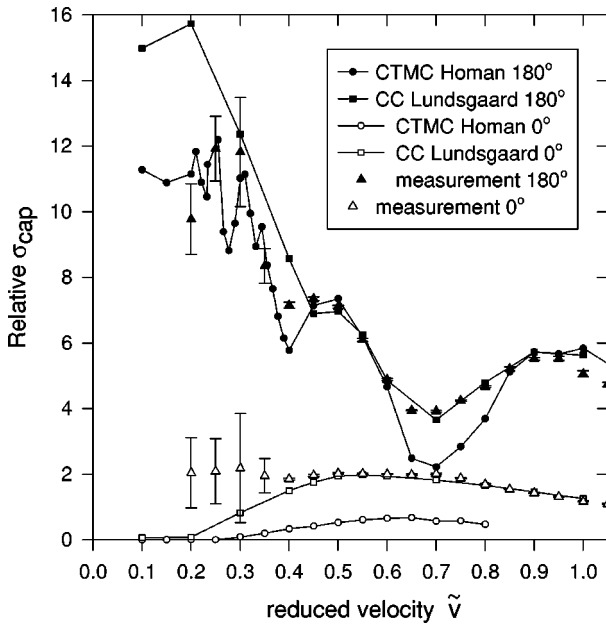


FIG. 5. Measured  $\sigma_{\text{cap}}(180^\circ)$  (solid triangles) and  $\sigma_{\text{cap}}(0^\circ)$  (open triangles) for  $K^+$  or  $Cs^+$  and  $Na(24 \text{ top})$  impact compared to both CTMC (circles) and CC (squares) calculations. The  $180^\circ$  measurements are normalized to the theories at  $\tilde{v} = 0.9$ . The normalization of experimental data at  $0^\circ$  follows from that for  $180^\circ$  and the measured ratios in Fig. 4. The approximately fourfold shortfall of the CTMC calculation at  $0^\circ$  is visible here (see the text).

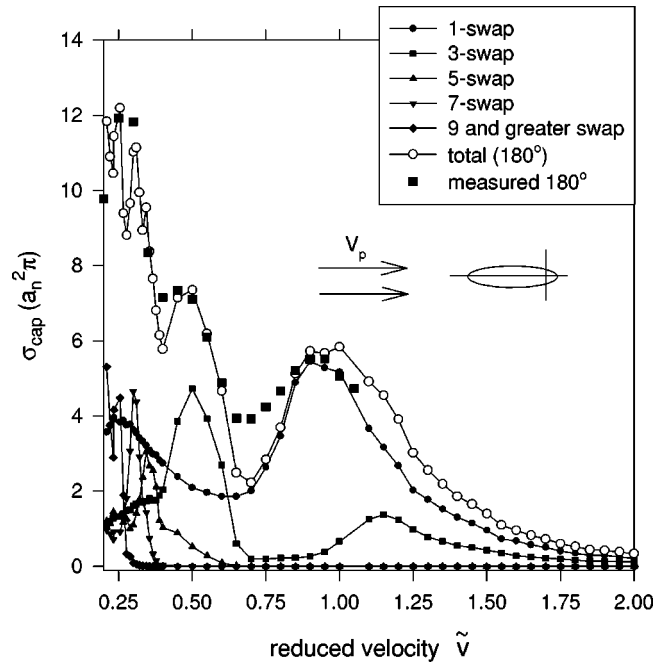


FIG. 6. Total CTMC capture cross section versus  $\tilde{v}$  for  $\theta = 180^\circ$  shown as open circles. The contributions of the one-, three-, five-, seven-, nine-, and greater-swap capture cross sections are also shown. The measured relative capture cross section is shown as solid squares for comparison, normalized to the CTMC result at  $\tilde{v} = 0.9$ .

cross section and a decreasing small one. It is better to compare the calculations directly with the measured relative cross sections for interpretation of the structure. In Fig. 5 the measured relative capture cross sections from  $Cs^+$  and  $K^+$  impacts on an upstream-directed ( $180^\circ$ , solid triangles) and a downstream-directed ( $0^\circ$ , open triangles) electron distribution are compared to the quantum (squares) and classical (circles) calculations. The  $180^\circ$  measurement is normalized to the CTMC calculation at  $\tilde{v} = 0.9$  and the relative scale for  $0^\circ$  measurements is then set by the measured ratios shown in Fig. 4. Both the measurement and the calculations show a broad peak near  $\tilde{v} = 0.9$  for the  $180^\circ$  plots shown as solid markers. The measurement and the calculations all have a similar minimum near  $\tilde{v} = 0.7$  and then a small shoulder around  $\tilde{v} = 0.5$ . At lower reduced velocities our greatest measured relative capture cross section was at  $\tilde{v} = 0.25$ . Both the classical and the quantal calculations have maxima near this reduced velocity. It is clear that the structure seen in the measurement of  $\sigma(180^\circ)$  is present in the calculations and may be understood in the context of the classical theory.

To gain further insight into the origin of the structure seen in the measurement, we separate the classical calculation into contributions of odd- $n$  swaps as was done in Refs. [5,14–17]. Figure 6 shows the total CTMC capture cross section as open circles, where each datum represents 40 000 trajectories, and statistical error bars are smaller than the marks. There is a structure seen in the cross section near  $\tilde{v} = 1, \frac{1}{2}, \frac{1}{3}$ , and  $\frac{1}{4}$ . The contributions of the one-swap (solid dots), three-swap (filled squares), five- and seven-swap (filled triangles), and nine-swap capture cross sections seem to be the underlying causes of the structure seen in the total capture cross

section in Fig. 6. These peaks mark the onset, for decreasing ion speeds, of each odd- $n$ -swap contribution to the total capture cross section as the electron passes many times between the two slowly approaching ions before being captured by the projectile ion. The close-coupling measurement shows a structure similar to both the measurement and the CTMC calculation.

In Fig. 5 the open symbols are the capture cross sections for  $\theta=0^\circ$ . Here the charge cloud is directed downstream and the CTMC capture cross section (open circles) is almost entirely due to one-swap contributions (contributions of swaps are not shown). This is not surprising since for there to be a three- or greater- $n$ -swap contribution, the electron's trajectory would have to pass near the two receding ions twice or more before becoming bound to the projectile. However, before the electron is likely to encounter the projectile at all in this configuration, the projectile ion itself will have moved past the target ion. It is unlikely that the electron would be scattered *back* and then be scattered *forward* again to overtake the advancing projectile. One-swap capture is more likely, for the electron would only need to move into the potential well of the passing projectile ion for those portions of its orbit spent nearly parallel to the ion's velocity. This is a mechanism of direct capture resulting from a velocity match of the electron and the projectile. There is a broad maximum in the downstream capture cross section near  $\tilde{v}=0.7$ . This has a classical interpretation as the velocity matching between the ion and the mean speed of the electron during its trajectory between peri- and apocenter.

The deviation of the measured downstream-directed relative capture cross section (open triangles in Fig. 5) from the calculations (open circles and squares) at low velocity may be the difference between Na and H (both theories assumed a hydrogenic target) or experimental error. More data will be needed for  $0.10 \leq \tilde{v} \leq 0.40$  to determine whether the  $0^\circ$  and  $180^\circ$  capture cross sections have more structure than can currently be resolved. Furthermore, the shortfall of the CTMC calculation relative to the CC calculation in the  $0^\circ$  target configuration (which is the source of the fourfold disagreement of the CTMC calculation that was removed by normalization in Fig. 4) is apparent here. It may be the result of ignoring differences between the Na(24 top) and H(24 top) states or the modeling of the 24 top Stark state classically by a single highly eccentric ellipse whose major axis is aligned *exactly* at  $0^\circ$  instead of averaging over the cone of angles suggested by the wave function in Fig. 3.

## V. DISCUSSION AND CONCLUSIONS

We have established that electron capture depends strongly on the position, not merely the momentum, of the electron in the collision complex of target and projectile for  $\tilde{v} \leq 1$ . It has also been shown that classical odd- $n$ -swap contributions to the total capture cross section can account for the strong variations of cross section  $\sigma(180^\circ)$  with velocity that are seen in the measurements. The close-coupling calculations are in good agreement with the  $180^\circ$  measurements and also reveal the peaks and shoulders near  $\tilde{v}=0.25, 0.5$ , and 1.0.

A similar structure was seen in earlier work of MacAdam *et al.* [5] and Hansen *et al.* [1], where capture by a singly charged alkali-metal ion from Na(24*d*) and Na(25*s*) showed peaks in the relative capture cross section at reduced velocities of 0.5 and 0.8. In both measurements the peak at  $\tilde{v}=0.5$  was shown classically to be a three-swap contribution to the total capture cross section and the peaks found in both measurements near  $\tilde{v}=0.8$  can be attributed to a one-swap contribution to the classically calculated capture cross section. The only difference between the classical modeling of the targets then and now was that the Na(24 top,  $m=0$ ) in the present work had a fixed Runge-Lenz vector, directed parallel or antiparallel to the ion beam direction, while the Na(24*d*,  $m=0$ ) had a randomly directed Runge-Lenz vector and most of the capture was found to be from the Runge-Lenz vector directed nearly parallel or antiparallel to the ion-beam direction. It was this classical study of the capture cross section versus the Runge-Lenz vector direction for a given beam energy that led the authors to study charge transfer from these extreme Stark states.

The next step in this work is to understand how the capture cross section for these collisions evolves as the electron distribution is swung from  $\theta=0^\circ$  to  $180^\circ$  at a given  $\tilde{v} \leq 1.0$ . A separate paper will address this task.

## ACKNOWLEDGMENTS

This research was supported in part by the Division of Chemical Sciences, Office of Basic Energy Sciences, Office of Energy Research, U.S. Department of Energy; the Research Corporation; and the NSF under Grant No. PHY-9704544. We are grateful for helpful discussions with T. Ehrenreich and E. Horsdal-Pedersen. We thank J.-C. Aguilar, W.L. Fuqua III, J.L. Horn, and G. Porter for help with the apparatus.

- 
- [1] S. B. Hansen, L. G. Gray, E. Horsdal-Pedersen, and K. B. MacAdam, *J. Phys. B* **24**, L315 (1991).
- [2] Th. Wörmann, Z. Roller-Lutz, and H. O. Lutz, *Phys. Rev. A* **47**, R1594 (1993).
- [3] S. B. Hansen, T. Ehrenreich, E. Horsdal-Pedersen, K. B. MacAdam, and L. J. Dubé, *Phys. Rev. Lett.* **71**, 1522 (1993).
- [4] T. Ehrenreich, J. C. Day, S. B. Hansen, E. Horsdal-Pedersen, K. B. MacAdam, and K. S. Mogensen, *J. Phys. B* **27**, L383 (1994).
- [5] K. B. MacAdam, J. C. Day, J. C. Aguilar, D. M. Homan, A. D. MacKellar, and M. J. Cavagnero, *Phys. Rev. Lett.* **75**, 1723 (1995).
- [6] O. P. Sorokina, D. M. Homan, O. P. Makarov, and K. B. MacAdam, *Bull. Am. Phys. Soc.* **42**, 1033 (1997).
- [7] J. C. Day, B. D. DePaola, T. Ehrenreich, S. B. Hansen, E. Horsdal-Pedersen, Y. Leontiev, and K. S. Mogensen, *Phys. Rev. A* **56**, 4700 (1997).
- [8] J. H. V. Lauritsen *et al.*, *J. Phys. B* **29**, 1093 (1996).
- [9] D. Doweck *et al.*, *Phys. Rev. Lett.* **64**, 1713 (1990).
- [10] N. F. Mott and H. S. W. Massey, *The Theory of Atomic Col-*

- lisions (Clarendon, Oxford, 1933).
- [11] J. Pascale, R. E. Olson, and C. O. Reinhold, *Phys. Rev. A* **42**, 5305 (1990).
- [12] J. Wang and R. E. Olson, *Phys. Rev. Lett.* **72**, 332 (1993).
- [13] J. Wang, R. E. Olson, K. Cornelius, and K. Tökési, *J. Phys. B* **29**, L537 (1996).
- [14] D. M. Homan, M. J. Cavagnero, and D. A. Harmin, *Phys. Rev. A* **51**, 2075 (1995).
- [15] D. M. Homan, M. J. Cavagnero, and D. A. Harmin, *Phys. Rev. A* **50**, R1965 (1994).
- [16] D. M. Homan, M. J. Cavagnero and D. A. Harmin, in *Two-Center Effects in Ion-Atom Collisions*, edited by T. J. Gay and A. F. Starace (AIP, New York, 1994), p. 281.
- [17] D. M. Homan, Ph.D. dissertation, University of Kentucky, 1997 (unpublished).
- [18] S. Bradenbrink, H. Reihl, Th. Wörmann, Z. Roller-Lutz, and H. O. Lutz, *J. Phys. B* **27**, L391 (1994).
- [19] S. Bradenbrink, H. Reihl, Z. Roller-Lutz, and H. O. Lutz, *J. Phys. B* **28**, L133 (1995).
- [20] M. F. V. Lundsgaard, Z. Chen, C. D. Lin, and N. Toshima, *Phys. Rev. A* **51**, 1347 (1995).
- [21] M. F. V. Lundsgaard, N. Toshima, Z. Chen, and C. D. Lin, *J. Phys. B* **27**, L611 (1994).
- [22] M. F. V. Lundsgaard, N. Toshima, and C. D. Lin, *J. Phys. B* **29**, 1045 (1996).
- [23] U. Thumm (unpublished).
- [24] M. Machholm and C. Courbin, *J. Phys. B* **29**, 1079 (1996).
- [25] S. E. Nielsen *et al.*, *J. Phys. B* **28**, 5295 (1995).
- [26] E. Sidky and C. D. Lin, *Bull. Am. Phys. Soc.* **42**, 1027 (1997).
- [27] L. H. Thomas, *Proc. R. Soc. London, Ser. A* **114**, 561 (1927).
- [28] R. Shakeshaft and L. Spruch, *Rev. Mod. Phys.* **51**, 369 (1979).
- [29] K. B. MacAdam, D. M. Homan, O. P. Makarov, and O. P. Sorokina, *Proceedings of the 14th International Conference on the Application of Accelerators in Research and Industry* (AIP, New York, 1997), p. 79.
- [30] L. D. Landau and E. M. Lifshitz, *Quantum Mechanics: Non-Relativistic Theory* (Pergamon, New York, 1958).
- [31] M. F. V. Lundsgaard and C. D. Lin, *Bull. Am. Phys. Soc.* **40**, 1270 (1995).
- [32] M. F. V. Lundsgaard, Ph.D. dissertation, Kansas State University, 1995 (unpublished).
- [33] R. M. Drisko, Ph.D. dissertation, Carnegie Institute of Technology, 1955 (unpublished).
- [34] B. H. Bransden and M. R. C. McDowell, *Charge Exchange and the Theory of Ion-Atom Collisions* (Clarendon, Oxford, 1992).
- [35] D. P. Hodgkinson and J. S. Briggs, *J. Phys. B* **9**, 255 (1976).
- [36] E. Horsdal Pedersen, J. V. Mikkelsen, J. Vaaben, and K. Taulbjerg, *Phys. Rev. Lett.* **41**, 1541 (1978).
- [37] G. V. Avakov, L. D. Blokhintsev, A. S. Kadyrov, and A. M. Mukhamedzhanov, *J. Phys. B* **25**, 213 (1992).
- [38] D. R. Schultz, C. O. Reinhold, and P. S. Krstić, *Phys. Rev. Lett.* **78**, 2720 (1997).
- [39] J. P. Hansen, L. Kochbach, S. A. Synnes, J. B. Wang, and A. Dubois, *Phys. Rev. A* **57**, R4086 (1998).
- [40] J. Horn, D. M. Homan, C.S. Hwang, W. L. Fuqua III, and K. B. MacAdam, *Rev. Sci. Instrum.* (to be published).
- [41] D. M. Homan, O. P. Makarov, K. B. MacAdam, M. F. V. Lundsgaard, C. D. Lin, and N. Toshima (unpublished).
- [42] D. A. Harmin, *Phys. Rev. A* **44**, 433 (1991).
- [43] R. N. Zare, *Angular Momentum: Understanding Spatial Aspects in Chemistry and Physics* (Wiley, New York, 1988).
- [44] Heat Wave, 765 Calabasas Road, Watsonville, CA 95076 (formerly known as Spectra Mat).
- [45] T. F. Gallagher, *Rydberg Atoms* (Cambridge University Press, New York, 1994).
- [46] K. B. MacAdam *et al.*, *Phys. Rev. A* **4**, 4661 (1986).
- [47] One could make a distinction between a classical trajectory study such as this one, in which a single ellipse was taken to represent the initial state, and one in which all classical orbital parameters, major-axis directions, etc., are appropriately distributed in intervals to correspond to quantum-mechanical states. The latter approach is referred to generally as the classical-trajectory Monte Carlo (CTMC) approach, but the terms CT and CTMC will be used interchangeably here. In our CT calculations for the 24 top state only the dynamically indeterminate initial position of the electron in its Keplerian orbit and the impact-parameter vectors of incident ions were averaged. The full CTMC approach is represented, e.g., by [11].
- [48] W. Fritsch and C. D. Lin, *Phys. Rep.* **202**, 1 (1991).
- [49] A. Bommier, D. Delande, and J. C. Gay, in *Atoms in Strong Fields*, edited by C. A. Nicolaides *et al.* (Plenum, New York, 1990), p. 155.
- [50] N. Toshima and C. D. Lin, *Phys. Rev. A* **46**, 2564 (1992).